Daytime Cycle of Low-Level Clouds and the Tropical Convective Boundary Layer in Southwestern Amazonia

C. STRONG, J. D. FUENTES, AND M. GARSTANG

Department of Environmental Sciences, University of Virginia, Charlottesville, Virginia

A. K. BETTS

Atmospheric Research, Pittsford, Vermont

(Manuscript received 18 May 2004, in final form 19 February 2005)

ABSTRACT

During the wet season in the southwestern Amazon region, daytime water transport out of the atmospheric mixed layer into the deeper atmosphere is shown to depend upon cloud amounts and types and synoptic-scale velocity fields. Interactions among clouds, convective conditions, and subcloud-layer properties were estimated for two dominant flow regimes observed during the 1999 Tropical Rainfall Measuring Mission component of the Brazilian Large-Scale Biosphere–Atmosphere (TRMM-LBA) field campaign. During daytime the cloud and subcloud layers were coupled by radiative, convective, and precipitation processes. The properties of cloud and subcloud layers varied according to the different convective influences of easterly versus westerly lower-tropospheric flows. The most pronounced flow-regime effects on composite cloud cycles occurred under persistent lower-tropospheric flows, which produced strong convective cloud growth with a near absence of low-level stratiform clouds, minimal cumulative attenuation of incoming solar irradiance (~25%), rapid daytime mixed-layer growth (>100 m h^{-1}), and boundary layer drying (0.22 g kg^{-1} h^{-1}), high convective velocities (>1.5 m s^{-1}), high surface buoyancy flux (>200 W m^{-2}), and high latent heat flux (600 W m^{-2}) into cloud layer. In contrast, persistent westerly flows were less convective, showing a strong morning presence of low-level stratiform genera (>0.9 cloud amount), greater cumulative attenuation of incoming solar irradiance (~47%), slower mixed-layer growth (<50 m h^{-1}) with a slight tendency for mixed-layer moistening, and a delayed peak in the low-level cumuliform cloud cycle (2000 versus 1700 UTC). The results reported in this article indicate that numerical models need to account for cloud amounts and types when estimating water vapor transport to the cloud layer.

1. Introduction

Two key objectives of the National Aeronautics and Space Administration's (NASA) Tropical Rainfall Measuring Mission (TRMM) (Simpson et al. 1988) are to define the vertical features of convection in the tropical atmosphere using satellite-borne radar and to quantify the associated distribution of latent heating. As part of the ground validation program for the TRMM satellite during the 1999 January–February wet season, the TRMM Large-Scale Biosphere–Atmosphere (TRMM-LBA) experiment was conducted in the Rondônia region of southwestern Brazil to provide a detailed resolution of convection over the interior of a tropical continent. The TRMM-LBA field campaign featured a comprehensive set of collocated instrument platforms, including micrometeorological towers, tethered balloons, rawinsondes, atmospheric profilers, surface radars, airborne radars, and a precipitation network. The TRMM-LBA campaign, in parallel with the Wet-Season Atmospheric Mesoscale Campaign (WETAMC-LBA), produced the most comprehensive dataset ever collected over the continental Tropics (Silva Dias et al. 2002).

Initial analyses of TRMM-LBA low-level (850–700 hPa) wind field data revealed synoptic-scale oscillations between easterly and westerly flow regimes that influenced the dynamics of convection over Rondônia (Rickenbach et al. 2002; Herdies et al. 2002) and nearby

Corresponding author address: Dr. J. D. Fuentes, Department of Environmental Sciences, 291 McCormick Road, Clark Hall, University of Virginia, Charlottesville, VA 22904.
E-mail: jf6s@virginia.edu

regions of South America (Petersen et al. 2002). Two flow regimes dominated the region during the TRMM-LBA field campaign. The lower-tropospheric westerly and easterly wind regimes were associated with the presence (westerly) or the absence (easterly) of "stationary frontal systems" extending into the deep Tropics along the South Atlantic convergence zone (SACZ) (Rickenbach et al. 2002). The mean position of the SACZ off of the Brazilian coast was heavily influenced by Amazon convection (Figueroa et al. 1995), and further variability was introduced by baroclinic wave activity originating in the extratropical Pacific Ocean (Liebmann et al. 1999). The easterly–westerly distinction was a reliable proxy for convection frequency, intensity, and vertical extent. Additionally, the observed synoptic flows had important implications for the spatial and temporal distributions of latent heating. Over Rondônia, the westerly flow regime included a shallower, cooler, and moister subcloud layer (Betts et al. 2002b), lower concentrations of cloud condensation nuclei (Williams et al. 2002), a relatively large fraction of stratiform rainfall, and weak convection nearly devoid of lightning (Halverson et al. 2002). In contrast, the easterly regime exhibited larger convective available potential energy (CAPE), larger convective inhibition (CIN), more strongly electrified storm systems with deeper radar reflectivity cores (Petersen et al. 2002), higher convective rain rates (Anagnostou and Morales 2002; Rickenbach 2004), larger raindrop radii (Carey et al. 2001; Tokai et al. 2002), stronger and deeper lower-tropospheric wind shear (Halverson et al. 2002), enhanced tilting of updraft cores, faster vertical air motion, and faster vertical mass transport (Cifelli et al. 2002). In general, the enhanced dynamical forcing of the easterly flow conditions contributed to the propagation of squall lines and mesoscale instabilities from the east South American coast (Silva Dias and Ferreira 1992; Garstang et al. 1994; Cohen et al. 1995) to the Amazon basin (Petersen et al. 2002).

Low-level clouds influence the amount of solar irradiance reaching the surface, and vertical fluxes of mass and energy. Tropical cumulonimbi, in particular, can act as effective conduits in the transport of mass and energy between the surface and deeper troposphere (Riehl and Malkus 1958; Garstang et al. 1988; Scala et al. 1990; Greco et al. 1994). Several observational and modeling studies have linked the type and amount of low-level clouds to variability in water mass flux (Yanai et al. 1973; Nitta 1975; Nicholls and Lemone 1980; Nicholls et al. 1982; Penc and Albrecht 1987), and related processes such as vertical motions (Bunker 1952; Emmitt 1978), spatial moisture gradients (Albrecht et al. 1985), and irradiance-induced buoyancy effects (Deardorff 1980; Fravalo et al. 1981; Caughey et al. 1982; Slingo et al. 1982; Brost et al. 1982; Nicholls 1984). Little work has been done, however, to define and quantify how cloud types and amounts influence the vertical transports of energy and mass within the tropical continental atmospheric boundary layer. Such information is relevant for improving the algorithms that are employed to verify the diabatic heating provided by the TRMM satellite, such as the Goddard Cumulus Ensemble (GCE) model (Tao et al. 1999). Improved physical understanding and model parameterizations are also required to represent a realistic diurnal cycle of precipitation in numerical forecast models over Amazonia (e.g., Bechtold et al. 2004).

In this manuscript we investigate the relationship between cloud amount and type obtained during TRMM-LBA and associated boundary layer thermodynamics to address three research goals. First, the daytime cycles of low-level stratiform and cumuliform clouds are established for each of the synoptic-flow regimes identified during the TRMM-LBA. Second, for each synoptic-flow regime, we investigate the relationship between mixed-layer thickness, mixed-layer potential temperature, mixed-layer humidity, free-convection velocity, precipitation statistics, and the turbulent fluxes of water vapor, energy, and solar irradiance. Third, for the different TRMM-LBA synoptic-flow regimes the ratios of the water vapor flux at the top of the mixed layer to the surface flux are computed to obtain a measure of water vapor transport efficiency from the surface to the free atmosphere.

2. Site characteristics and field measurements

Measurements were made at a pasture site located near Ouro Preto d'Oeste, Rondônia, Brazil (10°45′S, 62°22′W), during the wet season months of January and February 1999. Situated to the south of the Amazonian rainforest, the measurement site is part of a reasonably flat, 250-km^2 deforested region dominated by short grass (*Brachiaria brizantha*) with isolated palm and hardwood trees. A collocated micrometeorological flux tower, tethersonde system, and rawinsonde measurements were made to provide datasets with coordinated temporal and vertical resolution. Half-hourly turbulent fluxes of momentum (τ), latent heat (LE), sensible heat (H), and buoyancy were derived from turbulence measurements made at the frequency of 10 Hz using an eddy covariance system consisting of a sonic anemometer and infrared gas analyzer. Vertical profiles of pressure, temperature, relative humidity (RH), and horizontal wind speed and wind direction were measured with a tethersonde system consisting of a 30-m^3 balloon,

instrument sonde (Vaisala, Inc., Boulder, Colorado), and an onboard data acquisition system. A hydraulic winch was used to raise and lower the tethersonde at 1 m s^{-1} from 10 m above the surface to a maximum height of 1500 m at the nominal times of 0300, 0600, . . . , 2400 UTC (local standard time plus 4 h). The onboard data acquisition system recorded values every 2 s, producing measurements with a maximum vertical resolution of 2 m. Visual observations of cloud type (e.g., cumulus, stratus, altostratus) and cloud cover in eighths were recorded at the time of each tethersonde flight. Rawinsondes, equipped with global positioning system technology (VIZ, Inc., Philadelphia, Pennsylvania), were launched in coordination with the tethered balloon flights to measure pressure, temperature, RH, wind speed, and wind direction in the atmospheric layer extending from the surface to 25 km. The resulting datasets underwent extensive calibration and correction (Betts et al. 2002a) to minimize possible systematic humidity biases (Halverson et al. 2002). Rainfall data were obtained with tipping-bucket rain gauges (model TB4, Campbell Scientific, Inc., Logan, Utah) at the flux tower site and from 40 gauges in four clusters located within 60 km of the tower site (Fig. 1). The data analysis that is reported here is restricted to the days for which concurrent visual cloud observations and tethered balloon data are available: 22 January–28 February. The data included in this study were obtained in the middle of a pasture field with a horizontally homogeneous fetch exceeding 15 km. Therefore, the energy fluxes and boundary layer thermodynamics apply principally to a source footprint with a radius of 15 km. The large-scale flow regimes identified with the rawinsonde wind information were confirmed with multipoint upper-air soundings (Betts et al. 2002b; Halverson et al. 2002) and radar measurements (Rickenbach et al. 2002).

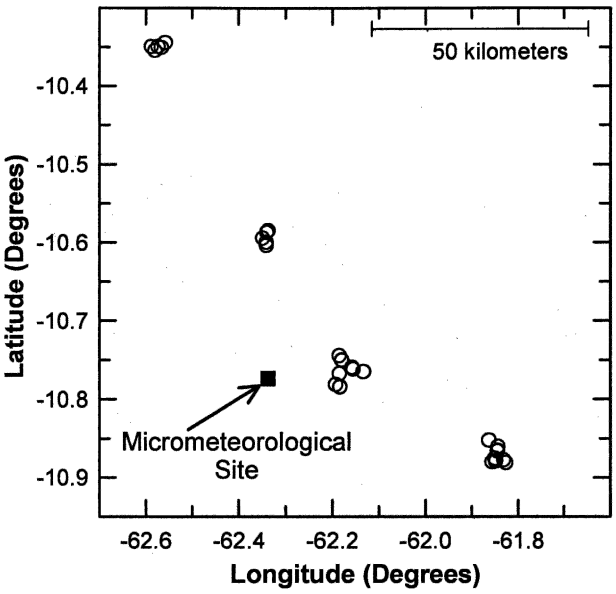

FIG. 1. Location of the network of 40 tipping-bucket rain gauges (open circles) and the micrometeorological measurement site in Rondônia, Brazil.

3. Methods

In the analyses described below, several quantities were derived from state variable measurements. The surface sensible ($F_{\theta 0}$) and latent heat (F_{q0}) fluxes were estimated from eddy covariance measurements using

$$F_{\theta 0} = \overline{\rho} C_p \overline{w'\theta'} \quad \text{and} \tag{1}$$

$$F_{q0} = \overline{\rho} L_v \overline{w'q'}. \tag{2}$$

The w and θ are the vertical velocity and potential temperature, respectively, and were measured with a sonic anemometer. The q represents the specific humidity and was measured with a gas analyzer (model LI-6262, LiCor, Inc., Lincoln, Nebraska). The quantities with primes ($'$) represent deviations from mean values, and quantities with overbars denote averages of the covariance over 30-min periods. The ρ, C_p, and L_v are the air density, specific heat capacity of dry air at constant pressure, and latent heat of vaporization, respectively. In humid environments, it is necessary to compute the surface virtual heat flux ($F_{\theta v0}$), defined in terms of $F_{\theta 0}$ and F_{q0} (Betts 1992), as in

$$F_{\theta v0} = F_{\theta 0} + 0.073 F_{q0}. \tag{3}$$

To obtain the average mixed-layer specific humidity ($\langle q \rangle_{\mathrm{ML}}$) and virtual potential temperature ($\langle \theta_v \rangle_{\mathrm{ML}}$), the tethered balloon measurements were integrated from the surface (denoted 0) to the top of the convective mixed layer (h) and normalized by the mixed-layer thickness, as in

$$\langle q \rangle_{\mathrm{ML}} = \frac{1}{h} \int_0^h q(z)\, dz \quad \text{and} \tag{4}$$

$$\langle \theta_v \rangle_{\mathrm{ML}} = \frac{1}{h} \int_0^h \theta_v(z)\, dz. \tag{5}$$

The h values were objectively determined from the second derivative of the tethersonde virtual potential temperature profile ($\partial^2\theta_v/\partial z^2$). The $\partial^2\theta_v/\partial z^2$ quantities exhibit pronounced and positive maximum values at h, which separates the nearly homogeneous mixed layer from the overlying stable transition layer.

The free-convective velocity (w_*) for individual atmospheric soundings was estimated to determine the

vertical velocity that was associated with thermals in the convective boundary layer. The w_* scales with the height (h) of the convective boundary layer and includes the influence of the buoyancy flux [which is defined here as the product of atmospheric buoyancy ($g/\langle\theta_v\rangle_{\mathrm{ML}}$) and the surface kinematic virtual heat flux ($\overline{w'\theta'_v}$)]. It is defined as

$$w_* = \left[h \frac{g}{\langle\theta_v\rangle_{\mathrm{ML}}} (\overline{w'\theta'_v}) \right]^{1/3}, \tag{6}$$

where g is the acceleration resulting from gravity. Willis and Deardorff (1974) originally established the validity of this scaling law. The moisture excess within thermals in the mixed layer was also determined. This quantify was derived based on the convective boundary layer parameter q_* as defined in

$$q_* = \frac{(\overline{w'q'})}{w_*}. \tag{7}$$

A key objective of this study is to relate the amount of water transport out of the mixed layer to cloud amounts and types. The latent heat fluxes (F_{qh}) at the top of the mixed layer (very close to cloud base) was estimated using water conservation budget methods that were developed for the vertically homogeneous mixed layer (Betts 1973, 1992; Tennekes 1973; Carson 1973; Deardorff et al. 1974; Barr and Betts 1997)

$$\overline{F_{qh}} = \overline{F_{q0}} - \langle\rho\rangle_{\mathrm{ML}} L_v \frac{\partial\langle q\rangle_{\mathrm{ML}}}{\partial t} h, \tag{8}$$

where $\langle\rho\rangle_{\mathrm{ML}}$ is the mixed layer air density, L_v is the latent heat of vaporization, and t is time. The temporal rate of humidity change ($\partial\langle q\rangle/\partial t$) was obtained from successive tethered balloon measurements, using relationship (4). This simplified budget equation assumes that the horizontal advection of humidity is negligible. For the TRMM-LBA project this was a reasonable assumption because the tethered balloon measurements were made over an extensive and homogenously flat terrain (Heitz 2000). The evaporation of falling precipitation in the mixed layer is a source term that contributes to $\partial\langle q\rangle/\partial t$, and so is a component of the derived flux F_{qh}. We minimized the impact of this effect on the present analysis by eliminating time periods of heavy precipitation.

To define the strength of convection that is associated with the identified synoptic regimes, CAPE and CIN were estimated. CAPE is the maximum energy that is available to an ascending air parcel, providing information about the buoyant stability of the atmosphere. High values (>1000 J kg^{-1}) of CAPE are associated with environments that are more prone to deep convection (Zipser and Lemone 1980; Jorgensen and LeMone 1989; Mapes and Houze 1992; Williams and Renno 1993). CIN is the energy that is needed to lift an air parcel pseudoadiabatically to its level of free convection. Higher values of CIN are associated with capping inversions atop the mixed layer that can delay convection, potentially resulting in increased updraft vigor once clouds erupt into the level of free convection (Fulks 1951; Carlson and Farrell 1982). CAPE and CIN can be expressed as

$$\mathrm{CAPE} = \int_{p_n}^{p_f} (\alpha_p - \alpha_e)\, \partial p \quad \text{and} \tag{9}$$

$$\mathrm{CIN} = -\int_{p_i}^{p_f} R_d (T_{v\text{-parcel}} - T_{v\text{-env}})\, \partial \ln p, \tag{10}$$

where α_e is the environmental-specific volume profile, α_p is the specific volume of air parcels moving upward moist adiabatically from the level of free convection, $T_{v\text{-parcel}}$ is the virtual temperature of the lifted air parcels, $T_{v\text{-env}}$ is the virtual temperature of the environment, p_f is the pressure at the level of free convection, p_n is the pressure at the level of neutral buoyancy, and p_i is the pressure at the level at which the parcel originated. In (10), p is atmospheric pressure; R_d is the ideal gas constant for dry air. CAPE and CIN values that are referenced here are also reported in Halverson et al. (2002).

a. Cloud data grouping

Daytime visual cloud observations were grouped into low-level cumuliform and low-level stratiform groups, where low-level indicates the low *étage* [cloud-base height below 2 km in the Tropics (World Meteorological Organization 1975)]. Cloud octa were converted to decimal values and grouped into 3-hourly blocks centered on the nominal times of 1100, 1400, . . . , 2300 UTC. One octa was assumed when a cloud type was mentioned without amount; average cloud amounts were produced when more than one sounding occurred within any 3-h time block; and cloud amounts were linearly interpolated between soundings when exactly one nominal observation time was missing between two soundings. This research focuses primarily on low-level cloud types because they are most closely coupled with the mixed layer. Nocturnal cloud patterns were not documented because of issues relating to nighttime visibility (e.g., Hahn et al. 1995). However, for the same time period and region in Brazil, and based on radar and satellite data analyses, Rickenbach (2004) reported the influences of nocturnal clouds on the weakening and delaying the onset of afternoon's convection.

b. Synoptic regime grouping

The easterly and westerly flow regimes identified for the TRMM-LBA data (Rickenbach et al. 2002; Petersen et al. 2002; Herdies et al. 2002) were used as a framework for grouping cloud, mixed-layer height, and precipitation data. The division of days used here follows the grouping employed by Betts et al. (2002b) after their reanalysis of the calibrated and corrected soundings. The easterly regime during 22–28 January will be referred to as E1, the westerly regime during 29 January–7 February is W1, the easterly regime during 8–21 February is E2, and the westerly regime during 22–28 February is W2.

c. Isohumes and scalar profiles

Time–height contours of specific humidity (isohumes) were developed by plotting micrometeorological tower, tethersonde, and rawinsonde humidity data against the decimal day of year on the abscissa and geopotential height on the ordinate. In the time–height data field, rawinsonde and tethersonde data were allowed to overlap below 1500 m. Contour lines were then fit to the time–height field at the spacing of 0.25 g kg^{-1}.

d. Clear-sky irradiance

Estimates of clear-sky irradiance were made as a reference with which to compare the measured incoming solar irradiance. Calculations were based on Beer's law and relationships for the position of the sun in the sky, and necessary quantities were included to account for Rayleigh scattering, permanent gas absorption, water vapor absorption, and aerosol scattering. Gu et al. (2001) provide full details concerning the required calculations.

4. Results and discussion

a. TRMM-LBA cloud cycles

This section presents the low-level cloud data in two parts. Section 4a(1) includes a synoptic-time-scale perspective by demonstrating the daytime mean low-level cloud amounts and vertical distribution of low-level specific humidity against the day of year. Section 4b(2) provides a diurnal-time-scale perspective by illustrating the regime composite cloud and mixed-layer data versus the time of day. The multiday composite averages of convective events within the identified flow regimes produce results that are representative of the 50 km × 50 km grid spacing used in global forecast models (Bechtold et al. 2004).

1) SYNOPTIC CLOUD CYCLE

Figure 2 provides the time series of daily average stratiform and cumuliform cloud amount, a time–height cross section of specific humidity q, and the corresponding time–height cross section of relative humidity. The E1 regime had the strong presence of cumuliform clouds (87% of the total low-level cloud amount), the near absence of stratiform clouds, and a persistent layer of <80% RH between 100 and 600 m (Fig. 2c). During the W2 case, by contrast, only 27% of the low-level cloud field was cumuliform, and the sky was dominated by stratiform clouds associated with nearly saturated composite conditions (>90% RH) from the surface to 1.5 km (Figs. 2a and 2c). The proceeding observations indicate that the consistent easterly direction of E1 flow supported a drier lower troposphere and a predominantly cumuliform low-level clouds, while the consistent westerly flow during W2 exhibited moister lower troposphere and increased stratiform cloud amounts. The dominance of stratiform clouds typically followed the occurrences of individual large mesoscale systems. Similar cloud distribution patterns were observed during the nighttime (Rickenbach 2004).

The two intervening regimes (W1 and E2) exhibited the inconsistent flow direction and were not consistently dominated by one low-level cloud type. Cumuliform clouds accounted for approximately 67% of the low-level cloud field for both W1 and E2. The W1 regime, classified as a "weak westerly" by Rickenbach et al. (2002), had a predominantly stratiform low-level cloud field only during the middle of the regime (day of year 33, 34; Fig. 2a). The 3 February (day of year 34) low-level stratiform peak was coincident with increasing specific and relative humidity below 2 km in Figs. 2b and 2c, and was indicative of flow oscillations (sign changes) in the 850–700-hPa zonal wind (e.g., Fig. 2a in Rickenbach et al. 2002; Fig. 5 in Halverson et al. 2002). Flow oscillations also contributed to humidity fluctuations in E2, providing a 3-day surge of stratiform cloud amount that was not replicated in E1.

2) REGIME DIURNAL CLOUD CYCLES

Figure 3 is organized into columns and rows, with each column corresponding to one of the four synoptic regimes. The rows provide the regime composite diurnal cycle of cloud amount (Figs. 3a–h) and cloud probability (Figs. 3i–t). One of the common characteristics across the four regimes is a reliable morning to midday cumuliform formation and stratiform destruction process. The probability and amount of low-level stratiform cloud decreased between 1100 and 1700 UTC in all regimes, and the probability and amount of low-

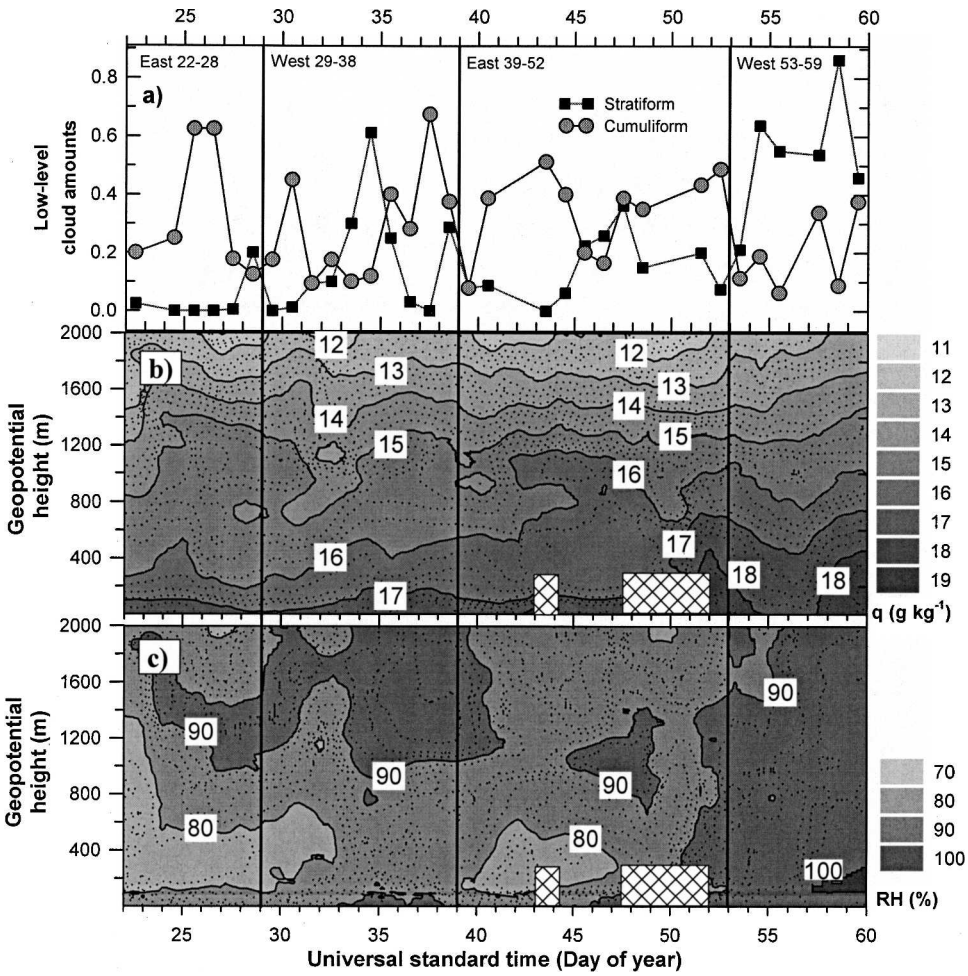

FIG. 2. (a) Mean daytime low-level stratiform and cumuliform cloud amounts vs day of year, and (b) isohumes of specific humidity and (c) relative humidity as a function of geopotential height and UTC day of year based on the composite of all data: tower (1 and 6 m), tethersonde (10–1200 m), and rawinsondes (300–2000 m). The vertical lines with labels delineate the synoptic periods referred to respectively as E1, W1, E2, and W2. The crosshatched areas indicate missing tethersonde data (Rondônia, Brazil, 1999).

level cumuliform clouds increased over the same time period in all regimes (Figs. 3a–1). The 1100–1700 UTC growth of cumuliform clouds was accompanied by an increase in the probability of cumulus congestus and cumulonimbus, while the concurrent decrease in stratiform clouds was accompanied by a decrease in the probability of stratus (Figs. 3m–t). Another common characteristic of all four regimes was a peak in cumuliform cloud probability near 1.0, at one or more observation times, together with a high probability of cumulus congestus or cumulonimbus. The common cumuliform signal indicates that widespread convection persisted over the Amazon, even during consistent westerly flow (Rickenbach et al. 2002; Cifelli et al. 2002; Carvalho et al. 2002; Petersen et al. 2002).

The diurnal pattern of stratiform cloud amount and probability clearly distinguished E1 from W2 (Fig. 3a versus Fig. 3d). In contrast, E2 and W1 had similar diurnal cloud patterns (Figs. 3b and 3f versus Figs. 3c and 3g), in part because E2 was less convectively charged than E1. Both E1 and E2 had high CAPE (Table 1) and a 1.0 probability of low-level cumuliform clouds within the 3 h centered on 1700 UTC (Figs. 3i and 3k), but their diurnal cumuliform cycles differed—a contrast that is explained, in part, by the lower CIN during E2 (Table 1), which allowed for an earlier initiation of deep convection (nonzero probability of cumulus congestus as early as 1100 UTC, Fig. 3o). By contrast, the high CIN in E1 capped strongly fueled convection and delayed the formation of cumulus congestus until 1700 UTC (Fig. 3m), after which time the low-level cumuliform cloud amount remained steady

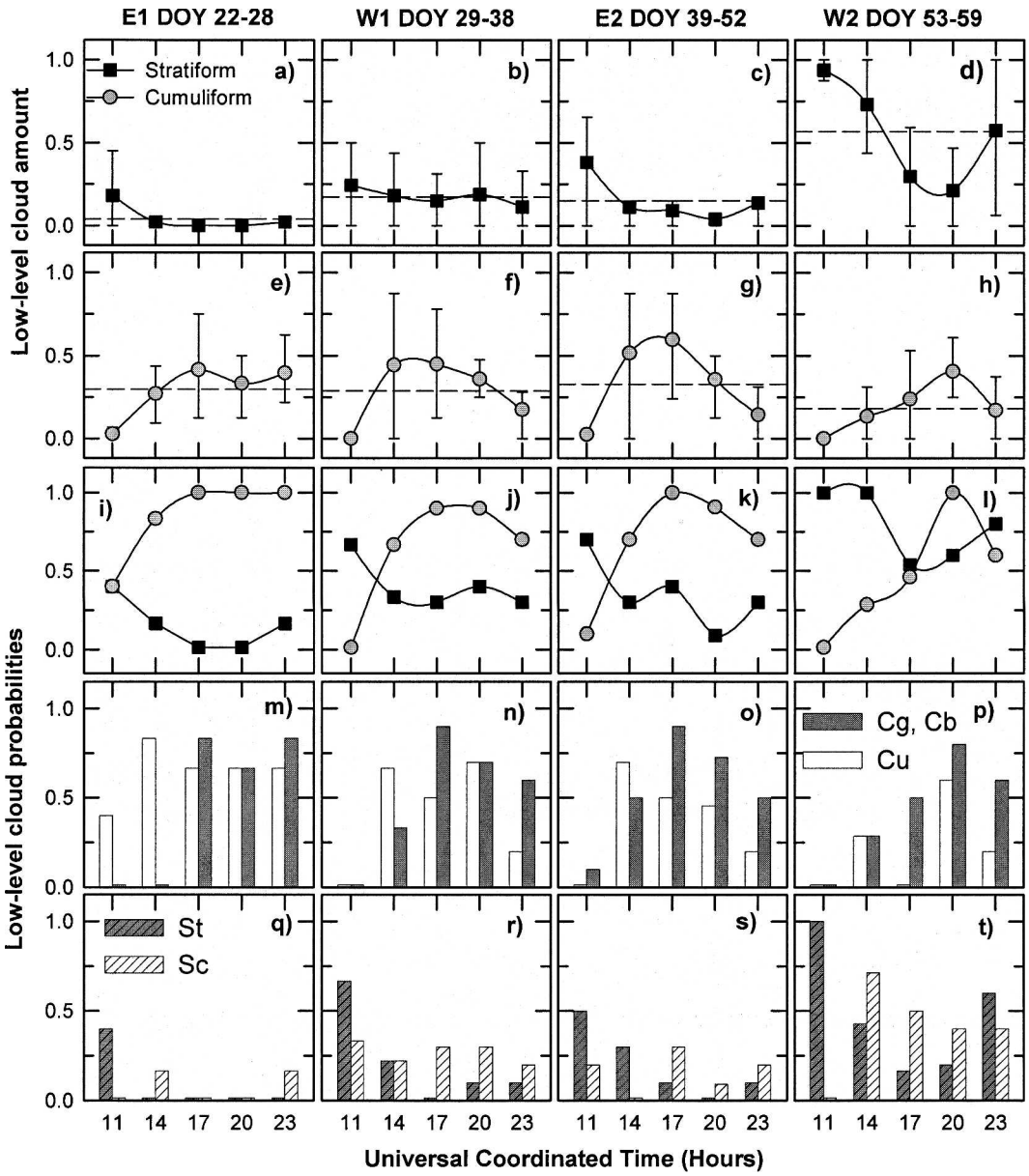

FIG. 3. Ensemble diurnal cycle of (a)–(d) low-level stratiform cloud amount, (e)–(h) low-level cumuliform cloud amount, (i)–(l) low-level stratiform and cumuliform probability of occurrence, and (m)–(t) probability of specific low-level cumuliform and stratiform cloud types. Data are in 3-hourly groups positioned over their central times (e.g., data over the 14 tick were collected between 1230 and 1530 UTC). Error bars on (a)–(h) span the interquartile range (25th–75th percentile) of each 3-hourly data group. Each column shows data for one regime as indicated at the top of the figure (Rondônia, Brazil, 1999).

near 0.4 and the probability of cumulus congestus or cumulonimbus remained near 0.85 (Figs. 3e and 3m). The delay in the formation of cumulus congestus can be explained by the convective systems that occurred the previous night. These nocturnal convective systems contributed to cooling and drying of the lower atmosphere, and to reduced morning solar irradiance resulting from the leftover stratiform clouds (Rickenbach 2004). The capped, strongly fueled convection during E1 suggests a more explosively released cloud field (Fulks 1951; Carlson and Farrell 1982)—a result that is consistent with the observed peak lightning flash rates, mean convective rain rates, stratiform rain fraction, and the classification of E1 as being the most "convectively vigorous" TRMM-LBA campaign regime (Halverson et al. 2002).

TABLE 1. CAPE and CIN values for easterly and westerly flow regimes observed in the Rondônia region of southwestern Brazil during Jan–Feb 1999.

Halverson et al. (2002) regime	CAPE* (J kg^{-1})	CIN* (J kg^{-1})	Regime used here
Easterly 1: 20–26 Jan	1504	−35	E1 (22–28 Jan)
Neutral: 27 Jan–8 Feb	1125	−19	W1 (29 Jan–7 Feb)
Easterly 2: 9–22 Feb	1530	−21	E2 (8–21 Feb)
Westerly 2: 23–28 Feb	1165	−11	W2 (22–28 Feb)

* Data from Halverson et al. (2002).

b. Cloud interactions with the subcloud layer

Clouds can modify the atmospheric layer from the surface to cloud base via convective circulations and the buoyant production of turbulence (e.g., Bunker 1952; Emmitt 1978; Nicholls and Lemone 1980). Although in situ measurements of cloud and subcloud turbulent fluxes were not made during TRMM-LBA, cloud-enhanced vertical velocities were evidenced by radar-based measurements of hydrometeors (Cifelli et al. 2002), and the composite effects of convective downdrafts were evidenced by changes in the properties of the subcloud layer (Betts et al. 2002b). Section 4b(1) shows how the diurnal cycle of the vertical fluxes of buoyancy, moisture, irradiance, mixed-layer scaling parameters, and precipitation varied with the synoptic-flow regimes and their associated cloud patterns. In section 4b(2), mixed-layer properties, such as thickness and specific humidity, are examined across the four flow regimes.

1) DIURNAL CYCLE OF MIXED-LAYER FLUXES AND PRECIPITATION

Figure 4 is organized into columns and rows, with each column corresponding to one of the four synoptic regimes. The first row of panels (Figs. 4a–d) shows the diurnal cycles of solar irradiance flux ($K\downarrow$) and buoyancy flux ($F_{\theta v}$). The gradual decrease in solar irradiance flux and buoyancy flux during the field campaign (Figs. 4a–d) paralleled the increase in stratiform cloud amount documented in section 4a(1), evidencing the influence of clouds on the mixed-layer energy cycle. The second row of panels in Fig. 4 shows latent heat flux at the surface (surface F_{q0}) and at the top of the mixed-layer height [F_{qh} from (8)]. The several missing F_{qh} values are most often associated with a precipitation disturbance. Peak F_{qh} events that are shown in Figs. 4e–h suggest that, in addition to modulating irradiance and available buoyant energy, cumuliform clouds may affect F_{qh}, the vapor flux out of the mixed layer, via the cloud-base buoyant production of vertical motion. During E2, for example, two individual F_{qh} values exceeded 600 W m^{-2} (Fig. 4g) and coincided with visual observations of deep convective clouds (cumulus congestus and/or cumulonimbus). The F_{qh} value of 600 W m^{-2} during W2 (Fig. 4h) occurred on 23 February (day of year 54), which was marked by a momentary clearing of low-level stratiform coverage after 1400 UTC and the rapid development of a 5/8 cumulus congestus deck. For all four flow regimes, the difference between ensemble F_{qh} (a least squares best fit, shown as a dashed line) and ensemble surface F_{q0} peaks in the range of 100–300 W m^{-2} (Figs. 4e–h). These values are comparable to the ensemble quantities reported for a tropical rain forest between 1400 and 1900 UTC by Martin et al. (1988).

Table 2 summarizes the mean ratio of the mixed-layer-top latent heat flux to surface latent heat flux (F_{qh}/F_{q0}) at three observation times for the four synoptic regimes. On average, F_{qh} tended to exceed surface F_{q0} during the daytime (grand mean $F_{qh}/F_{q0} \cong 1.20$), consistent with the mixed layer's composite tendency to dry following the onset of convection [section 4b(2)]. The highest mean F_{qh}/F_{q0} values ($\geq$1.4) were associated with easterly flow regimes, reflecting these regimes' more vigorously convective nature. Values of F_{qh}/F_{q0} in excess of 1.4 were comparable to quantities that were measured during the Amazon Boundary Layer Experiment (ABLE) IIa over a tropical forest during the dry season (~1.5; Martin et al. 1988). The mean F_{qh}/F_{q0} ratios prior to 1700 UTC (e.g., E1 Fig. 4e and Table 2) probably reflected the mixed layer's rapid growth, rather than any cloud-enhanced entrainment effects. However, the mean F_{qh}/F_{q0} ratios for the later part of the afternoon, when mixed-layer growth had slowed, indicated cloud-enhanced entrainment effects (e.g., 2000 UTC during E2, Fig. 4g and Table 2). Cumulus enhancement of mixed-layer mass flux was also present during E1 in the hours about 2000 UTC, but the number of estimates was limited to one because of the frequent convective rain disturbance.

The third row of Fig. 4 shows how convective velocity (w_*) and the moisture scaling parameter q_* varied across the four synoptic regimes. The high buoyancy flux ($F_{\theta v}$) and high CAPE in E1 (Table 1) supported vigorous thermals (high w_*) that produced intensely penetrative convection, and led to the quick decline of moisture excesses (q_*) into the afternoon (Fig. 4i). In contrast, the less convectively charged W1 and E2 supported moister thermals (q_*) with slower-moving thermals (w_*, Figs. 4j and 4k). The fourth row of Fig. 4 shows "nonzero rain rates" across the four regimes, calculated as the mean of the rain gauge clusters when and where precipitation was nonzero. Analogous to the

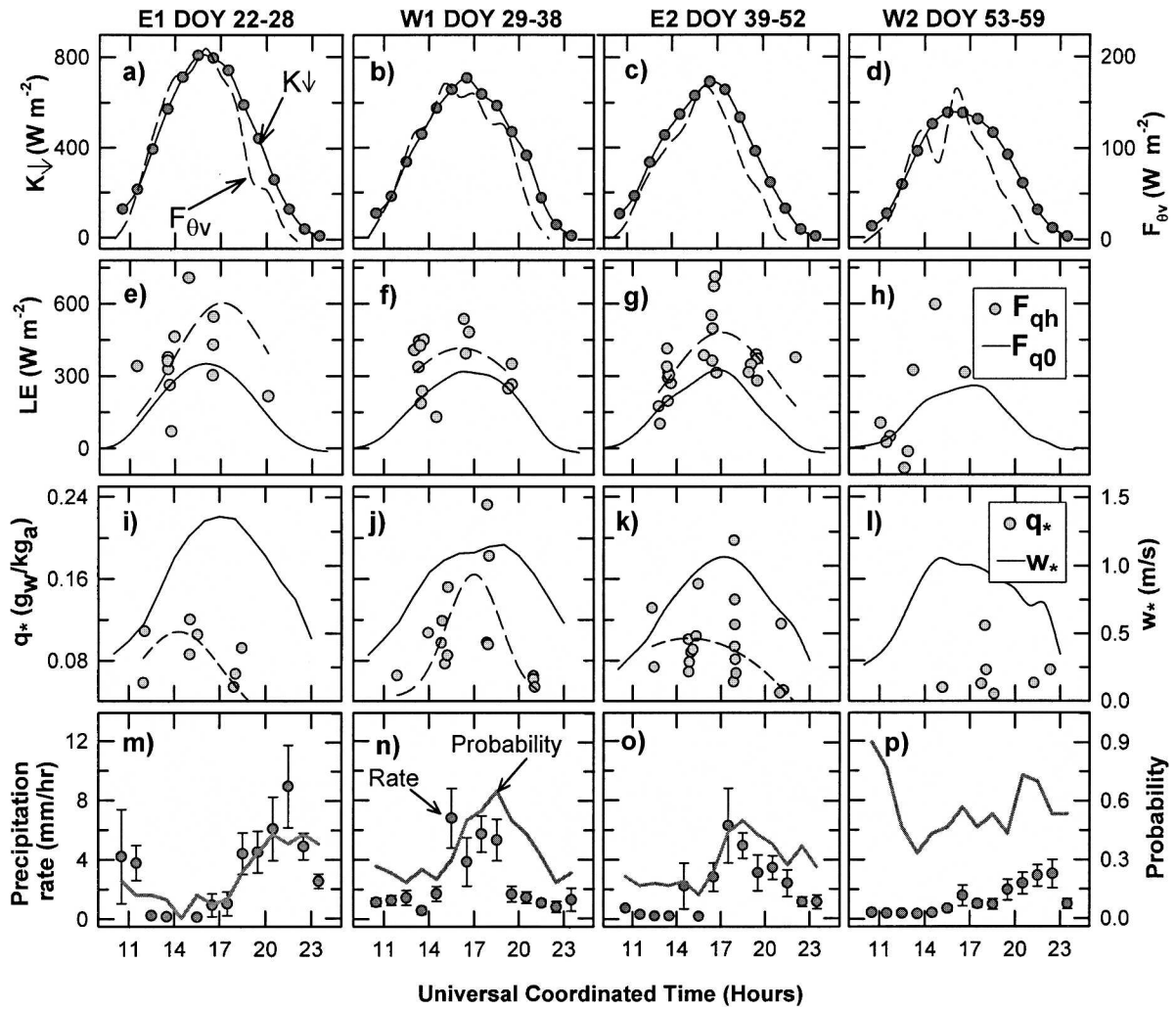

FIG. 4. (a)–(d) Mean incoming solar irradiance ($K\downarrow$) and buoyancy flux ($F_{\theta v}$, (e)–(h) mixed-layer-top latent heat flux (F_{qh}) and hourly surface latent heat flux (F_{q0}) with a Gaussian best fit to F_{qh} shown as a dashed line where data are sufficient, (i)–(l) mean convective velocity (w_*) and the moisture scaling parameter q_* with a Gaussian best fit to q_* shown as a dashed line where data are sufficient, (m)–(p) the hourly mean rain rate with standard error when precipitation was nonzero (circles with error bars), and the probability of rain (gray lines). Each column shows data for one regime as indicated at the top of the figure (Rondônia, Brazil, 1999).

"conditional" rain rates that are derived from radar analysis (e.g., Halverson et al. 2002), the nonzero rain-rate statistic contrasts the fast rain rates that are produced by isolated convective cells against the slower, more widespread precipitation rates associated with stratiform systems. The precipitation pattern in E1 showed a clearly convective signature in which rain was relatively rare prior to 1700 UTC, after which time rain rates rapidly increased and culminated in the highest nonzero rain rates of the campaign (Fig. 4m). The pre-

TABLE 2. Mean and standard deviations (σ) of the ratio of mixed-layer-top latent heat flux to surface latent heat flux (F_{qh}/F_{q0}) for 3-h blocks of time during the four TRMM-LBA synoptic-flow regimes. Dashed standard deviations indicate only one available measurement, and dashed ratio values indicate zero available measurements (Rondônia, Brazil, 1999).

Start time (UTC)	E1		W1		E2		W2	
	$\overline{F_{qh}/F_{q0}}$	σ	$\overline{F_{qh}/F_{q0}}$	σ	$\overline{F_{qh}/F_{q0}}$	σ	$\overline{F_{qh}/F_{q0}}$	σ
1400	1.12	0.29	1.11	0.32	1.17	0.35	1.19	0.30
1700	1.40	0.53	1.23	0.18	1.18	0.36	0.74	—
2000	1.06	—	1.04	0.13	1.43	0.35	—	—

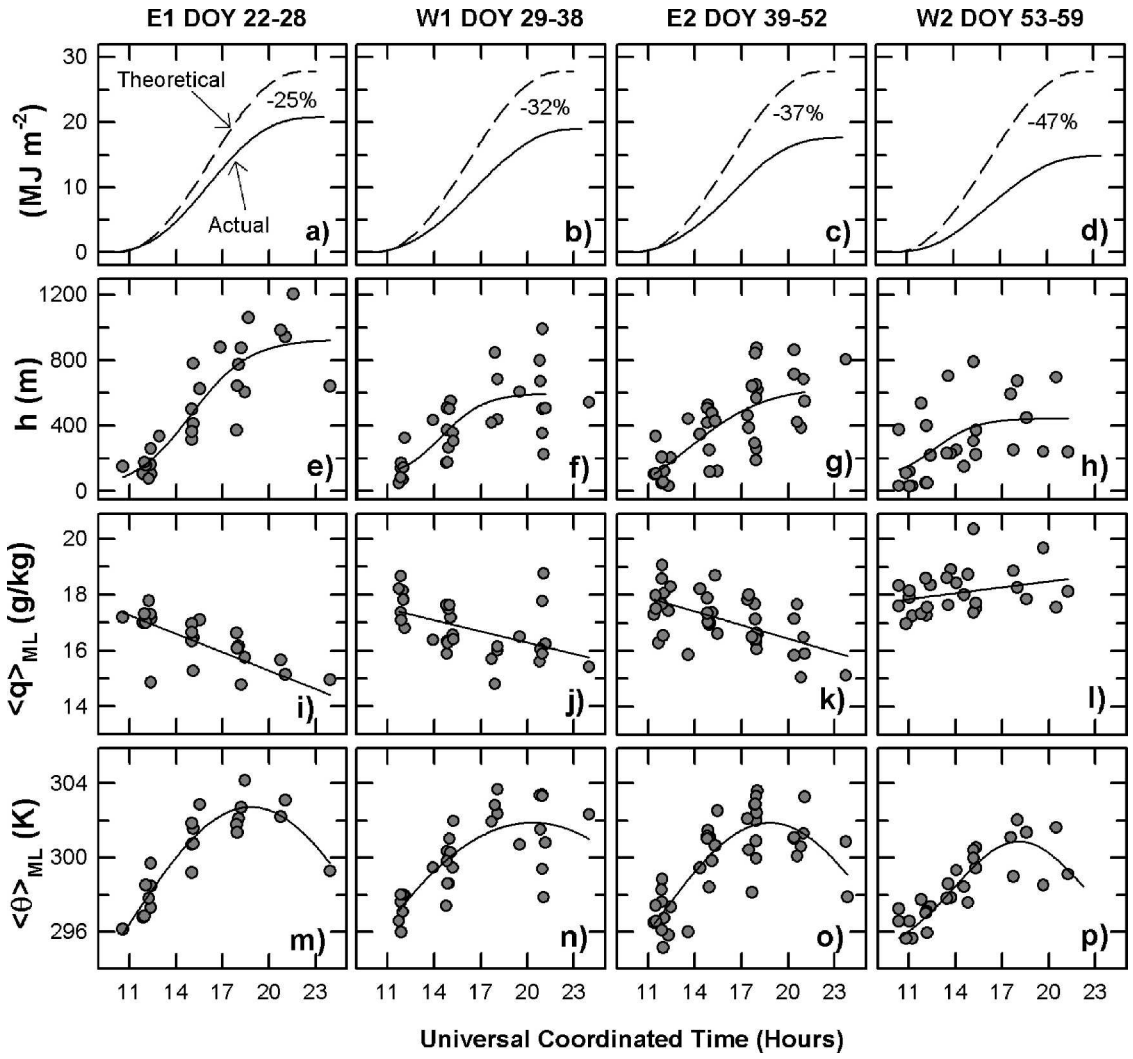

FIG. 5. (a)–(d) Diurnal integrated incoming solar irradiance ($K\downarrow$, solid lines) with dashed lines showing the integration of theoretical cloud-free irradiance, (e)–(h) mixed-layer thickness with sigmoidal least squares best-fit lines, (i)–(l) mixed-layer mean specific humidity $\langle q \rangle_{ML}$ with linear least squares best-fit lines, and (m)–(p) mixed-layer mean potential temperature $\langle \theta \rangle_{ML}$ with Gaussian least squares best-fit lines. Each column shows data for one regime as indicated at the top of the figure (Rondônia, Brazil, 1999).

cipitation rates for W1 and E2 (Figs. 4n and 4o) peaked close to 1700 UTC in concert with the probability of deep convective clouds [section 4a(2)], but were weaker than the E1 rates. The W2 rain pattern was clearly stratiform: nonzero rain rates were about one-third the rates of the first three regimes, and it was almost always raining at 1100 UTC (>0.9 probability) at a very slow rate (<1 mm h^{-1}, Fig. 4p).

2) DIURNAL CYCLE OF MIXED-LAYER THICKNESS, HUMIDITY, AND TEMPERATURE

Figure 5 is organized into columns and rows, with each column corresponding to one of the four synoptic regimes. The first row (Figs. 5a–d) compares the integrated measured solar irradiance with the theoretical clear-sky irradiance, showing the increasing deficit of incoming energy associated with increasing stratiform cloud amounts. As the field campaign progressed, the decrease in integrated solar irradiance contributed to progressively slower composite mixed-layer growth and a shallower mixed-layer thickness at 2000 UTC (Figs. 5e–h), progressively slower composite mixed-layer drying (Figs. 5i–k), shifting to moistening in Fig. 5l, and progressively slower composite mixed-layer warming (Figs. 5m–p). The fastest (steepest slope) composite mixed-layer drying occurred during the convectively charged E1 regime (Fig. 5i). This result was consistent

with the E1 regime's relatively fast composite mixed-layer growth, relatively rapid dry air entrainment, and larger vapor flux divergence [section 4b(1)]. The mixed layer in the stratiform W2 regime showed a slight moistening with time, perhaps caused by evaporation of the weak steady stratiform rain into the mixed layer, as well as the reduced convective activity and dissipation of dense stratiform clouds.

5. Summary and conclusions

Distinct cycles in low-level cloudiness, the convective boundary layer, and cloud growth and boundary layer to cloud-layer detrainment were observed in the low-latitude continental location of the TRMM-LBA field campaign. Such changes contrast strongly with the more steady-state conditions observed over the open tropical oceans (Garstang and Fitzjarrald 1999). Persistent westerly or easterly flow in the lower troposphere produced convective regimes with distinct diurnal patterns of low-level clouds and subcloud-layer processes and properties. During the first easterly regime El, convective instability contributed to establishing a predominantly (87%) cumuliform low-level cloud field and high sustained probabilities (~0.80) of cumulus congestus and cumulonimbus from midday through sunset. Reduced attenuation of the incoming solar irradiance and the generation of convective circulations contributed to the warmest composite mixed layer (303 K), the highest mean half-hourly convective velocity (1.36 m s^{-1}), the highest mean half-hourly buoyancy flux (>200 W m^{-2}), and the highest composite latent heat flux out of the mixed layer (600 W m^{-2}). The vigorously convective thermals and flux processes caused rapid mixed-layer growth (>100 m h^{-1}) and drying (0.22 g kg^{-1} h^{-1}), resulting in the deepest (900 m) composite mixed layer. This especially convective El cloud field experienced the highest composite nonzero rain rates (>9 mm h^{-1}) of the TRMM-LBA field campaign.

In contrast to easterly regime, the westerly flow (W2) regime exhibited a predominantly stratiform cloud field and the greatest net attenuation of the daily cumulative incoming solar irradiance (47%). These conditions were associated with a cooler and moisture subcloud layer with weaker peak composite buoyancy flux (~150 W m^{-2}) and lower composite convective velocities. Composite mixed-layer growth was slower during W2, resulting in a shallower peak composite mixed-layer thickness (~450 m) and a tendency for specific humidity to be stable or increasing. The W2 regime also featured a stabilizing, predominantly stratiform precipitation signature with relatively high probabilities of rain and low nonzero rain rates.

The intervening flow regimes (W1 and E2) are subject to fluctuations in lower-tropospheric wind direction and humidity, and were intermediate in terms of cumuliform versus stratiform dominance. In a comparison of the two easterly regimes, E2 had increased levels of episodic stratiform genera, and a reduced cumuliform fraction of the total low-level cloud field (0.68 for E2 versus 0.87 for E1). Regime E2 also had lower CIN than E1, allowing an earlier discharge of deep convection, a somewhat weaker composite vapor flux divergence and mixed-layer drying, an earlier and weaker peak in the composite nonzero precipitation rate, and an earlier decline of cumulus congestus.

The E2 regime F_{qh}/F_{q0} ratio mean >1.4 around 2000 UTC indicated that vertical turbulent motions at the base of cumuliform clouds enhanced water mass flux through the upper boundary of the mixed layer, particularly after 1700 UTC when mixed-layer growth had slowed. Differences in mixed-layer growth, convective velocities, surface buoyancy, and cloud-layer entrainment of latent heat flux, together with the sensitivity of F_{qh}/F_{q0} to the presence of convective clouds and the observed variability of F_{qh}/F_{q0} with changing synoptic regimes raise concerns on how well numerical models can parameterize the boundary layer and precipitating clouds over the continental Tropics.

Acknowledgments. NASA provided support to carry out the field investigations included in this study under grant NAG5-9654 to the University of Virginia. NASA also supported the data analyses through grant NAG5-9856. We thank Dr. Ramesh Kakar, NASA Program Scientist, for his continued support. Author CS was partly supported under a National Science Foundation Graduate Research Fellowship. AKB received supported from NSF under grant ATM-9988618 and NASA under grant NAS5-11578. Jeff M. Sigler and Ryan Heitz from the University of Virginia and Gilberto Fisch, Julio Tota da Silva, and Paolo Jorge Oliveira from Centro Técnico Aerospacial, São José dos Campos, assisted with the field measurements. Three anonymous reviewers provided excellent comments to improve the original manuscript.

REFERENCES

Albrecht, B. A., R. S. Penc, and W. H. Schubert, 1985: An observational study of cloud-topped mixed layers. *J. Atmos. Sci.,* **42,** 800–822.

Anagnostou, E. N., and C. A. Morales, 2002: Rainfall estimation from TOGA radar observations during LBA field campaign. *J. Geophys. Res.,* **107,** 8068, doi:10.1029/2001JD000377.

Barr, G., and A. K. Betts, 1997: Radiosonde boundary layer budgets above a boreal forest. *J. Geophys. Res.,* **102,** 29 205–29 212.

Bechtold, P., J.-P. Chaboureau, A. Beljaars, A. K. Betts, M. Köhler, M. Miller, and J.-L. Redelsperger, 2004: The simulation of the diurnal cycle of convective precipitation over land in a global model. *Quart. J. Roy. Meteor. Soc.,* **130,** 3119–3137.

Betts, A. K., 1973: Non-precipitating cumulus convection and its parameterization. *Quart. J. Roy. Meteor. Soc.,* **99,** 178–196.

——, 1992: FIFE atmospheric boundary layer budget methods. *J. Geophys. Res.,* **97,** 18 523–18 531.

——, J. H. Ball, and J. D. Fuentes, 2002a: Calibration and correction of LBA/TRMM Abracos pasture site merged dataset. ORNL DAAC, 28 pp. [Available online at ftp://daac.ornl.gov/data/lba/physical_climate/Betts, or on CD-ROM from Atmospheric Research, 58 Hendee Lane, Pittsford, VT 05763.]

——, J. D. Fuentes, M. Garstang, and J. H. Ball, 2002b: Surface diurnal cycle and boundary layer structure over Rondônia during the rainy season. *J. Geophys. Res.,* **107,** 8065, doi:10.1029/2001JD000356.

Brost, R. A., J. C. Wyngaard, and D. H. Lenschow, 1982: Marine stratocumulus layers. Part I: Mean conditions. *J. Atmos. Sci.,* **39,** 800–817.

Bunker, A. F., 1952: Measurements of the vertical water vapor transport and distribution within unstable atmospheric ground layers and the turbulent mass exchange coefficient. *Pap. Phys. Oceanogr. Meteor., Mass. Inst. Tech. and Woods Hole Oceanog. Inst.,* Vol. 12, No. 3.

Carey, L. D., R. Cifelli, W. A. Peterson, S. A. Rutledge, and M. A. F. Silva Dias, 2001: Characteristics of Amazonian rain measured during TRMM-LBA. Preprints, *30th Int. Conf. on Radar Meteorology,* Munich, Germany, Amer. Meteor. Soc., 682–684.

Carlson, T., and R. Farrell, 1982: The lid strength index as an aid in predicting severe local storms. *Natl. Wea. Dig.,* **8,** 27–39.

Carson, D. J., 1973: The development of a dry inversion-capped convectively unstable boundary layer. *Quart. J. Roy. Meteor. Soc.,* **99,** 450–467.

Carvalho, L. M. V., C. Jones, and M. A. F. Silva Dias, 2002: Intraseasonal large-scale circulations and mesoscale convective activity in tropical South America during the TRMM-LBA campaign. *J. Geophys. Res.,* **107,** 8042, doi:10.1029/2001JD000745.

Caughey, S. J., B. A. Crease, and W. T. Roach, 1982: A field study of nocturnal stratocumulus. II. Turbulence structure and entrainment. *Quart. J. Roy. Meteor. Soc.,* **108,** 125–144.

Cifelli, R., W. A. Petersen, L. D. Carey, S. A. Rutledge, and M. A. F. Silva Dias, 2002: Radar observations of the kinematic, microphysical, and precipitation characteristics of two MCSs in TRMM LBA. *J. Geophys. Res.,* **107,** 8077, doi:10.1029/2000JD000264.

Cohen, J. C. P., M. A. F. Silva Dias, and C. A. Nobre, 1995: Environmental conditions associated with Amazonian squall lines: A case study. *Mon. Wea. Rev.,* **123,** 3163–3174.

Deardorff, J. W., 1980: Cloud top entrainment instability. *J. Atmos. Sci.,* **37,** 131–146.

——, G. E. Willis, and D. K. Lilly, 1974: Comments on Betts. *Quart. J. Roy. Meteor. Soc.,* **100,** 122–123.

Emmitt, G. D., 1978: Tropical cumulus interaction with and modification of the subcloud region. *J. Atmos. Sci.,* **35,** 1485–1502.

Figueroa, S. N., P. Satyamurty, and P. L. D. Silva Dias, 1995: Simulations of the summer circulation over the South American region with an Eta coordinate model. *J. Atmos. Sci.,* **52,** 1573–1584.

Fravalo, C., Y. Fouquart, and R. Rosset, 1981: The sensitivity of a model of low stratiform clouds to radiation. *J. Atmos. Sci.,* **38,** 1049–1062.

Fulks, J. R., 1951: The instability line. *Compendium of Meteorology,* T. F. Malone, Ed., Amer. Meteor. Soc., 647–652.

Garstang, M., and D. R. Fitzjarrald, 1999: *Observations of Surface to Atmosphere Interactions in the Tropics.* Oxford University Press, 405 pp.

——, and Coauthors, 1988: Trace gas exchanges and convective transports over the Amazonian rain forest. *J. Geophys. Res.,* **93,** 1528–1550.

——, H. L. Massie Jr., J. Halverson, S. Greco, and J. Scala, 1994: Amazon coastal squall lines. Part I: Structure and kinematics. *Mon. Wea. Rev.,* **122,** 608–622.

Greco, S., J. Scala, J. Halverson, H. L. Massie Jr., W.-K. Tao, and M. Garstang, 1994: Amazon coastal squall lines. Part II: Heat and moisture transports. *Mon. Wea. Rev.,* **122,** 623–635.

Gu, L., J. D. Fuentes, M. Garstang, J. Tota, R. H. Heitz, J. Sigler, and H. H. Shugart, 2001: Cloud modulation of surface solar irradiance at a pasture site in southern Brazil. *Agric. For. Meteor.,* **106,** 117–129.

Hahn, C. J., S. G. Warren, and J. London, 1995: The effect of moonlight on observation of cloud cover at night, and application to cloud climatology. *J. Climate,* **8,** 1429–1446.

Halverson, J. B., T. Rickenbach, B. Roy, H. Pierce, and E. Williams, 2002: Environmental characteristics of convective systems during TRMM-LBA. *Mon. Wea. Rev.,* **130,** 1493–1509.

Heitz, R. H., 2000: Mixed layer budgets and entrainment rates of heat and water vapor over a deforested site in Amazonia. M.S. thesis, Department of Environmental Sciences, University of Virginia, 160 pp.

Herdies, D. L., A. Da Silva, and M. A. F. Silva Dias, 2002: Moisture budget of the bimodal pattern of the summer circulation over South America. *J. Geophys. Res.,* **107,** 8075, doi:10.1029/2001JD000997.

Jorgensen, D. P., and M. A. LeMone, 1989: Vertical velocity characteristics of oceanic convection. *J. Atmos. Sci.,* **46,** 621–640.

Liebmann, B., G. N. Kiladis, J. A. Marengo, T. Ambrizzi, and J. D. Glick, 1999: Submonthly convective variability over South American and the South Atlantic convergence zone. *J. Climate,* **12,** 1877–1891.

Mapes, B. E., and R. A. Houze, 1992: An integrated view of 1987 Australian monsoon and its mesoscale convective systems, Part I, Horizontal structure. *Quart. J. Roy. Meteor. Soc.,* **118,** 927–963.

Martin, C. L., D. Fitzjarrald, M. Garstang, A. P. Oliveira, S. Greco, and E. Browell, 1988: Structure and growth of the mixing layer over the Amazonian rain forest. *J. Geophys. Res.,* **93,** 1361–1375.

Nicholls, S., 1984: The dynamics of stratocumulus: Aircraft observations and comparisons with a mixed-layer model. *Quart. J. Roy. Meteor. Soc.,* **110,** 783–820.

——, and M. A. Lemone, 1980: The fair weather boundary layer in GATE: The relationship of subcloud fluxes and structure to the distribution and enhancement of cumulus clouds. *J. Atmos. Sci.,* **37,** 2051–2067.

——, ——, and G. Sommeria, 1982: The simulation of a fair weather marine boundary layer in GATE using a three dimensional model. *Quart. J. Roy. Meteor. Soc.,* **108,** 167–190.

Nitta, T., 1975: Observational determination of cloud mass flux distribution. *J. Atmos. Sci.,* **32,** 73–91.

Penc, R. S., and B. A. Albrecht, 1987: Parametric representation of heat and moisture fluxes in cloud-topped mixed layers. *Bound.-Layer Meteor.,* **38,** 225–248.

Petersen, W. A., S. W. Nesbitt, R. J. Blakeslee, R. Cifelli, P. Hein, and S. A. Rutledge, 2002: TRMM observations of intraseasonal variability in convective regimes over the Amazon. *J. Climate,* **15,** 1278–1294.

Rickenbach, T. M., 2004: Nocturnal cloud systems and the diurnal variation of clouds and rainfall in southwestern Amazonia. *Mon. Wea. Rev.,* **132,** 1201–1219.

——, R. N. Ferreira, J. Halverson, D. L. Herdies, and M. A. F. Silva Dias, 2002: Modulation of convection in the southwestern Amazon basin by extratropical stationary fronts. *J. Geophys. Res.,* **107,** 8040, doi:10.1029/2000JD000263.

Riehl, H., and J. S. Malkus, 1958: On the heat balance in the equatorial trough zone. *Geophysica,* **6,** 503–538.

Scala, J., and Coauthors, 1990: Cloud draft structure and trace gas transport. *J. Geophys. Res.,* **95,** 17 015–17 030.

Silva Dias, M. A. F., and R. N. Ferreira, 1992: Application of the linear spectral model to the study of Amazonian squall lines during GTE/ABLE 2B. *J. Geophys. Res.,* **97,** 20 405–20 419.

——, and Coauthors, 2002: Cloud and rain processes in a biosphere-atmosphere interaction context in the Amazon Region. *J. Geophys. Res.,* **107,** 8072, doi:10.1029/2001JD000335.

Simpson, J., R. F. Adler, and G. R. North, 1988: A proposed Tropical Rainfall Measuring Mission (TRMM) satellite. *Bull. Amer. Meteor. Soc.,* **69,** 278–295.

Slingo, A., R. Brown, and C. L. Wrench, 1982: A field study of stratocumulus, III: High resolution radiative and microphysical observations. *Quart. J. Roy. Meteor. Soc.,* **108,** 145–165.

Tao, W.-K., J. Simpson, C. H. Sui, C. L. Shie, B. Zhou, K. M. Lau, and M. Moncrieff, 1999: Equilibrium states simulated by cloud resolving models. *J. Atmos. Sci.,* **56,** 3128–3139.

Tennekes, H., 1973: A model for the dynamics of the inversion above a convective boundary layer. *J. Atmos. Sci.,* **30,** 558–567.

Tokai, A., A. Krueger, W. F. Krajewski, P. A. Kucera, and A. J. Pereira Filho, 2002: Measurements of drop size distribution in the southwestern Amazon basin. *J. Geophys. Res.,* **107,** 8052, doi:10.1029/2001JD000355.

Williams, E., and N. Renno, 1993: An analysis of the conditional instability of the tropical atmosphere. *Mon. Wea. Rev.,* **121,** 21–36.

——, and Coauthors, 2002: Contrasting convective regimes over the Amazon: Implications for cloud electrification. *J. Geophys. Res.,* **107,** 8082, doi:10.1029/2001JD000380.

Willis, G. E., and J. W. Deardorff, 1974: A laboratory model of the unstable planetary boundary layer. *J. Atmos. Sci.,* **31,** 1297–1307.

World Meteorological Organization, 1975: *Manual on the Observation of Clouds and Other Meteors*. Vol. I, *International Cloud Atlas,* WMO 407, 155 pp.

Yanai, M., S. Esbensen, and J. H. Chu, 1973: Determination of bulk properties of tropical cloud clusters from large scale heat and moisture budgets. *J. Atmos. Sci.,* **30,** 611–627.

Zipser, E., and M. A. Lemone, 1980: Cumulonimbus vertical velocity events in GATE. Part II: Synthesis and model core structure. *J. Atmos. Sci.,* **37,** 2458–2469.